A Multiscale Contrast Enhancement for Mammogram Using Dynamic Unsharp Masking in Laplacian Pyramid

Xiaoman Duan, Yingjie Mei, Shuyu Wu, Qingqing Ling, Genggeng Qin, Jianhui Ma,
Chaomin Chen, Hongliang Qi, Linghong Zhou, and Yuan Xu

Abstract—**Mammography is the first option for screening breast cancer. However, some lesions may be missed due to superimposition of breast parenchymal patterns/tissues. Current enhancement methods can highlight some specific tissues, but the edges are weakened or extra noise is added. For improving the solution, this paper proposed a multiscale contrast enhancement for mammogram using dynamic unsharp masking (UM) in Laplacian pyramid. Laplacian pyramid is utilized to preserve the fine structure at each scale. Dynamic UM is presented to adaptively enhance details and suppress noise simultaneously. The proposed method mainly consists of five steps: 1) downsample images; 2) calculate the weight of dynamic UM; 3) utilize dynamic UM enhancement for each scale image; 4) subtract the enhancement results for each scale image to acquire Laplacian pyramid images; and 5) restore the final enhanced image. To evaluate the proposed method qualitatively and quantitatively, one phantom and three clinical mammography cases were evaluated. Results showed the proposed method can provide much clearer details of the mammary gland. Quantitatively, information entropy and peak signal-to-noise ratio are increased by 0.96 and 3.89 at most compared with the state-of-the-art method. The proposed method has demonstrated that different types of regions are enhanced with the help of a regional adaptive evolution, which has great potential for adaptively enhancing the details and relatively suppressing the noise.**

Index Terms—**Dynamic unsharp masking (UM), Laplacian pyramid, mammogram enhancement.**

I. Introduction

BREAST cancer accounts for over 30% of deaths by cancer in women and approximately 1% of all deaths

worldwide [1]. To date, no effective method can prevent breast cancer due to its complex causes. Full field digital mammography, since it can detect cancer at an early stage, is more welcomed by the physicians [2]. Hence, the survival rate can be improved by a wide range of treatment options. However, several significant features related to breast cancer are rarely detected on mammograms due to the poor gray contrast of the image acquired by mammography, such as mass, calcifications, architectural distortion, asymmetries, intramammary lymph node, skin lesion, solitary dilated duct, etc. Specifically, the X-ray transmitting through the entire breast directly makes the structure superimposed and covered. Clinically, it is sometimes difficult to precisely locate irregular-shaped micro-calcifications and masses, as well as distinguishing between benign and malignant tumors. Therefore, improving the contrast of breast tissues and highlighting their structural information have a significant impact in the diagnosis of breast cancer, especially for patients with dense breast tissues [3]–[5].

Currently, enhancement approaches such as histogram equalization (HE) [6], [7], unsharp masking (UM) [2], [8]–[10], fuzzy sets (FSs) theory [11]–[13], and multiscale transformation [14]–[17] are common solutions for enhancing mammogram. Image enhancement through HE can improve image contrast by achieving a nearly uniform output of gray level distribution. However, that global operation cannot enhance small pixel differences among adjacent or superimposed breast tissues. High-frequency amplification is an efficient method that clarifies edges and details. UM is applied to enhance the edge details by adding high-frequency information to the original image based on the weight factor. UM has superior performance in enhancing the details of an image but amplifies noise and overshoots in the sharp regions at the moment. Various approaches have been developed to reduce the artifacts. Polesel *et al.* [8] employed an adaptive filter which divided an image into low-contrast and high-density components based on local neighborhood values; thereafter, the low, medium, and high weights were utilized to enhance the different areas. Deng [10] presented a novel tangent system based on a specific Bregman divergence, thereby enabling users to manually adjust two parameters and control the contrast and sharpness for the desired results. FSs models are very effective in removing noise without destroying the useful information of images. Deng *et al.* [12]
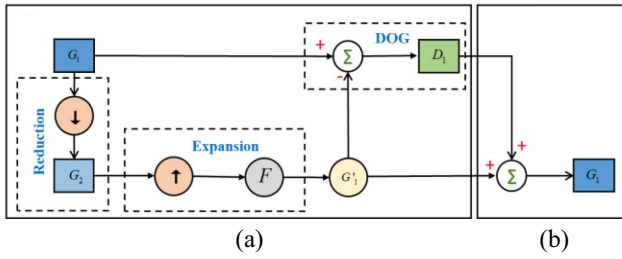
Fig. 1. (a) Image decomposition stage. (b) Image reconstruction stage.

presented an enhancement method based on intuitionistic FSs, which could improve the contrast and visual quality of abnormalities in mammograms. Multiscale transformation has proven to be a far more efficient method than regular unsharp-masking techniques [16]. Laine *et al.* [14] utilized the orientation and frequency selectivity of wavelet transforms to improve mammographic features contrast via localized contrast gain. Mencatini *et al.* [17] presented a method for mammogram enhancement and noise suppression using dyadic wavelet processing.

This paper proposed a multiscale contrast enhancement for mammogram using dynamic UM in Laplacian pyramid (LP_DUM). Being different from the conventional LP enhancement (LPE) and UM methods, the proposed method utilizes dynamic weight factors to adaptively enhance details and suppress noise. In particular, Laplacian decomposition is utilized to preserve the fine structure at each scale. Furthermore, the image global mean, neighborhood mean, and neighborhood variance are calculated to determine the weight of DUM for adaptively enhancing image by different degrees with the aid of a regional adaptive evolution.

The remainder of this paper is organized as follows. Section II contains a brief review of LP and a detailed description of the proposed DUM. Thereafter, the implementation of the proposed method is introduced in detail. Section III presents the experimental results. Section IV discusses a few related issues. Section V provides the conclusions.

II. MATERIALS AND METHODS

A. Laplacian Pyramid

LP was first proposed by Burt *et al.*, which performs multiscale decomposition of an image and obtains a Gaussian pyramid and Laplacian pyramid. Taking first-scale decomposition as an example, image deconstruction and image reconstruction stages are shown in Fig. 1.

The image deconstruction stage includes reduction, expansion, and the difference of Gaussian (DOG) step. In the reduction step, down-sampling ($\downarrow$) process is implemented on the original image G_1. Hence, the next scale image G_2 is acquired thereafter, which maintains the low-frequency information of G_1. In the expansion step, up-sampling ($\uparrow$) and Gaussian kernel F are applied upon G_2 to obtain the prediction image G'_1. In the DOG step, the Laplacian image D_1 is obtained through a difference operation between G_1 and G'_1. In reconstruction stage, G_1 can be acquired by adding G'_1

and D_1. It should be noted that Gaussian filtering process F, down-sampling ($\downarrow$) and up-sampling ($\uparrow$) here are just symbol representations. The mathematical equation and corresponding parameters of them will be cleared in Section II-C.

In most cases, G_2 will continue to deconstruct into lower scales via reduction step. Lastly, we can obtain a Gaussian pyramid that comprises a series of low-frequency images $(G_1, G_2, \ldots, G_{N+1})$ (assuming N times deconstruction) and an LP that consists of difference images $(D_1, D_2, \ldots, D_N)$. Later, the original image will be reconstructed layer by layer starting from lowest scale Gaussian image G_{N+1} and difference image D_N.

Liu *et al.* [18] developed an LPE algorithm by adding the Laplacian image D_n to the prediction image G'_n by a factor of k_n at each scale $n(n = N, \ldots, 2, 1)$. This process is performed in image reconstruction stage from the lowest scale to the upper until the image reconstruction is completed ($n = 1$). This algorithm can be formulated as follows:

$$G_n = G'_n + k_n D_n \tag{1}$$

where k_n is a weight factor that determines the proportion of the Laplacian image, that is, accounted in recovery processing. Different k_n indicates different degree of high frequency information of the image are enhanced.

B. Dynamic Unsharp Masking

Besides LPE, we proposed a novel DUM algorithm to simultaneously enhance the images at each scale images of LP. DUM is proposed based on UM. UM can be expressed as follows:

$$U = G + \lambda(G - G \cdot H_{\text{LP}}) \tag{2}$$

where G denotes the original image, function H_{LP} is a low-pass filter, U is the image after processed, and λ is a linear high-frequency weight factor to control how much to boost the high frequency. Compared with the traditional UM, DUM sets a dynamic weight factor $h(i, j)$ for each pixel (i, j) on the image to substitute the weight factor λ which is a constant for the whole image. The subscripts i and j are the ith row and jth column elements of breast image. DUM are defined through the following formula:

$$U = G + h(i, j)(G - G \cdot H_{\text{LP}}) \tag{3}$$

where $h(i, j)$ is defined for each pixel (i, j) as follows:

$$h(i, j) = \alpha \frac{\text{mean}}{\mu(i, j) + \log(\sigma(i, j))}. \tag{4}$$

The *mean* denotes the global gray average for the image, except for air component. $\mu(i, j)$ and $\sigma(i, j)$ are the neighborhood mean and neighborhood variance, respectively. The size of the neighborhood is set 11×11 to balance the computation efficiency and the enhancement effect. α is a constant weight factor of DUM like λ in UM. In general, rules of thumb and subjective evaluation are used for selecting α. The typical value of α in experiments substantially is 0.6 which maintains the details and none of artifacts increasing in mammogram
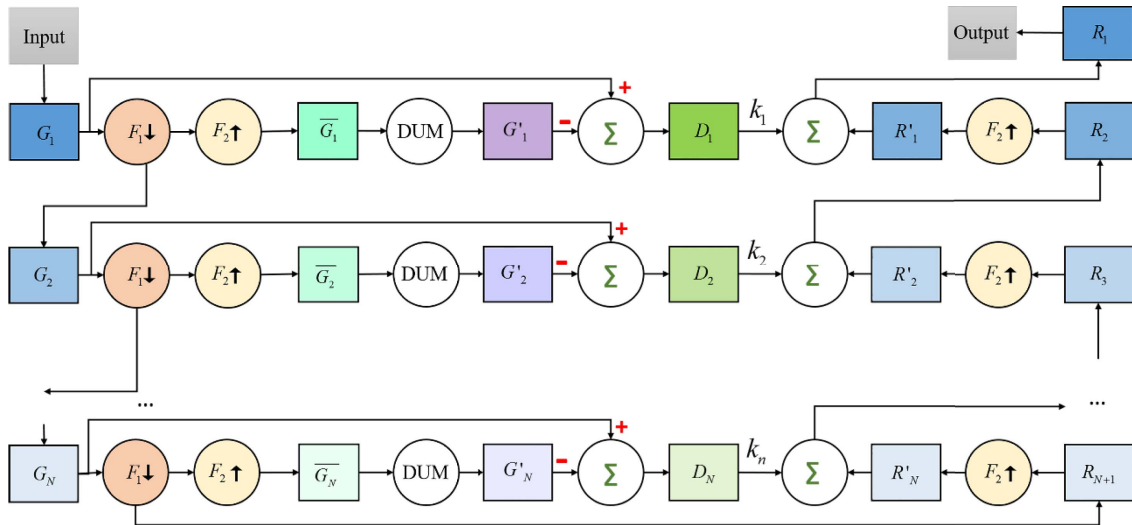
Fig. 2. Workflow of LP-DUM method.

enhancement. The primary function of logarithm on the variance is to ensure that there is still a certain enhancement effect when the variance is quite large.

At the edge of the skin, the $\sigma(i,j)$ is relatively large comparing to the other regions. Despite that, the value of $\log(\sigma(i,j))$ is relatively small. Then the effect of $\log(\sigma(i,j))$ in weighting factor $h(i, j)$ can be excluded from consideration. Therefore, for the processed pixel at the edge of the skin, $h(i, j)$ is mainly determined by $\mu(i,j)$ and *mean* value. In addition, $\mu(i,j)$ is less than *mean* value at the edge of the skin. Consequently, the weighting factor $h(i, j)$ is appropriately increased, thereby further enhancing the edge of the skin. For the pixel inside the breast, $\mu(i, j)$ is approximately equal to *mean*. The neighborhood where $\sigma(i, j)$ is relatively large will reduce $h(i, j)$. Thus, relative noise suppression is implemented. When $\mu(i, j)$ is larger than *mean*, such as in micro-calcifications region, the corresponding weight factor is reduced to avoid over-enhancement.

C. Implementation of the Workflow

Fig. 2 shows the workflow of proposed method including N layers of LP. G_1 is the input mammogram and R_1 is the final result after processed. First, the original image is processed with Gaussian filter and down-sampling ($\downarrow$) at a factor of 2 ($F_1 \downarrow$) iteratively to acquire Gaussian pyramid images G_N, which maintaining the basic structure of the original image

$$G_{n+1}(i,j) = \sum_{x=-2}^{2} \sum_{y=-2}^{2} w(x, y)G_n(2i - x, 2j - y)$$
$$n = 1, \ldots, N - 1 \tag{5}$$

where

$$w(x, y) = \frac{1}{2\pi\sigma^2} e^{-\frac{x^2+y^2}{2\sigma^2}}. \tag{6}$$

The parameter σ is applied to each image level. The smoothing effect of the filter increases by enlarging its value; however, high-frequency information is lost simultaneously. σ is chosen to be 1.6 typically [19]. The filter kernel $w(x, y)$ is typically selected to be a 5×5 pattern of weights in many literatures [16], [19], [20]. The Gaussian pyramids are generated by a sequence of smoothed image ($G_1, G_2, \ldots, G_{N+1}$).

The prediction image $\overline{G_n}$ is obtained by using expansion processing on the Gaussian pyramid images as described in the LP reconstruction stage. This procedure can be formulated as follows:

$$\overline{G_n}(i,j) = \sum_{x=-2}^{2} \sum_{y=-2}^{2} W(x, y)G_{n+1}((i - x)/2, (j - y)/2) \tag{7}$$

where $W(x, y)$ is the recovery filter, here, we suppose $W(x, y) = 4w(x, y)$ referencing [19].

Second, the weighting factor $h(i, j)$ of the prediction image is calculated to obtain the enhanced prediction image G'_n at each scale

$$G'_n(i,j) = \overline{G_n}(i,j) + h(i,j)\big(\overline{G_n}(i,j) - H_{\text{LP}}\overline{G_n}(i,j)\big). \tag{8}$$

H_{LP} can be any appropriate low-pass filter such as mean filter of 5×5.

The LP image D_n is the difference between the Gaussian pyramid image G_n and the matching scale enhanced image G'_n. Accordingly, D_n can be expressed as

$$D_n(i,j) = G_n(i,j) - G'_n(i,j). \tag{9}$$

In addition, the down-sampling image of the last scale Gaussian pyramid image G_N is considered the first recovery image R_{N+1}, which is calculated as follows:

$$R_{N+1}(i,j) = \sum_{x=-2}^{2} \sum_{y=-2}^{2} w(x, y)G_N(2i - x, 2j - y). \tag{10}$$

Thereafter, the first recovery image R_{N+1} recovers to the upper scale by up-sampling and filtering operation to obtain the up-sampling recovery image R'_n

$$R'_n(i,j) = \sum_{x=-2}^{2} \sum_{y=-2}^{2} W(x, y)R_{N+1}((i - x)/2, (j - y)/2). \tag{11}$$
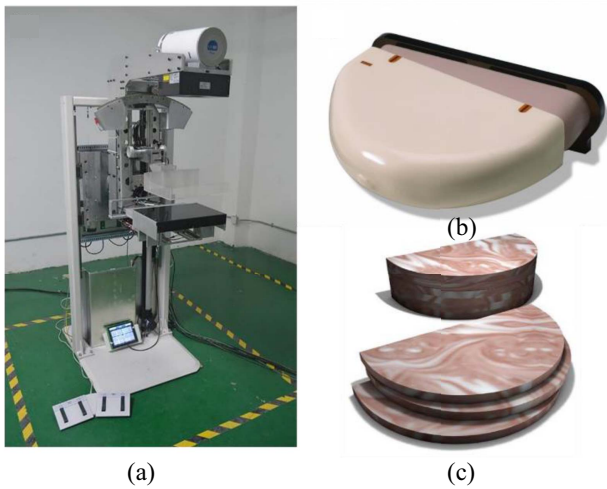
Fig. 3. Experimental materials. (a) Digital mammography system. (b) Physical shape of CIRS 011A. (C) Internal structures of CIRS 011A.

Lastly, the LP image D_n is linearly added to the up-sampling recovery image R'_n for the succeeding recovery

$$R_n(i, j) = R'_n(i, j) + D_n(i, j) \times k_n. \tag{12}$$

In the workflow, (11) and (12) are implemented iteratively to obtain the enhanced image R_1.

D. Data Acquisition

To verify the efficacy and efficiency of the proposed enhanced method, experiments are conducted using the quality control (QC) phantom (CIRS, Inc., USA) [21] data first. In general, these phantoms are often used for imaging quality analysis. They still can be evaluated the enhanced effect for images with sufficiently reflecting a real breast.

Data were acquired in the digital mammography system [see Fig. 3(a)], which was only used for research purposes. The tube voltage range changed from 25 to 32 kV. All mammograms were acquired on modern automatic exposure control mode with 40–60 mAs. The time of exposure is 400–600 ms, and the current of tube is 100 mA. The detector readout dimension is 3584×2816 with a pixel size of 0.07 mm $\times$ 0.07 mm at 4096 gray level. Fig. 3(b) shows the physical shape of the QC phantom and Fig. 3(c) displays the phantom internal structures. These structures comprise 50% fat with thickness of 4.5 cm and 50% simulated material of the glands.

The experiments with realistic breast data were also conducted. For intuitive understanding, three different types of breast images were chosen for display in this paper. It should be understood that although a few types of images were shown, our method is not limited to these images. The first type, heterogeneously dense breast, possessing numerous salivary ducts and limited fat, is considerably common in young women. The second type is breast with calcifications inside, whose distribution, shape, and number of high correlations with early breast cancer [22], [23]. The third type is breast with predominating fatty tissue, which often has noticeable salivary ducts but an unnoticeable edge profile. In this paper, the three realistic breast images were retrospectively collected

and anonymized for clinical research purposes. This paper did not involve new mammography of patients and, therefore, did not require approval of the local ethics committee. All patients provided written informed consent for their images to be used for research purposes and to be published. Original images, both phantom data and three typical realistic breast data, were acquired by only negative logarithmic transformation of projection data. Uniform distribution of gray scale in breast area without details highlighted makes precise diagnosis quite difficult.

UM in [10], LPE in [18], and the proposed method (i.e., LP_DUM) are separately used to enhance images.

To quantitatively evaluate the different enhancement performance, we utilized the index information entropy (IE) [24] to measure the enhanced contrast. Such effect is expressed as follows:

$$\text{IE} = -\sum_i \sum_j P(i, j) \log_2 P(i, j) \tag{13}$$

where

$$P(i, j) = \frac{f(i, j)}{\sum_i \sum_j f(i, j)}. \tag{14}$$

$P(i, j)$ denotes the probability of the pixel gray value $f(i, j)$ that accounts in the global gray value. The higher IE value is, the more details are preserved in the image.

In addition, peak signal-to-noise ratio (PSNR) are applied to assess the noise suppression of the proposed method. Given a reference image f and a test image g, both of size $M \times N$, the PSNR [25], [26] between f and g is defined by

$$\text{PSNR} = 10 \log_{10} \left(\frac{\max_f^2}{\text{MSE}} \right) \tag{15}$$

where MSE is given by

$$\text{MSE} = \frac{1}{MN} \sum_i \sum_j (f(i, j) - g(i, j))^2 \tag{16}$$

$\max_f$ denotes the maximum gray value of the reference image f. The PSNR value approaches infinity as the MSE approaches zero; this shows that a higher PSNR value provides a higher image quality.

III. RESULTS

A. Phantom Data

The processed results of phantom images by using the three methods are shown in Fig. 4. It can be seen that the whole contrast of processed image by LP_DUM is clearer and the lesion regions are easily discernible.

For better focus for the specific regions in the phantom images, four different cropped regions delineated by the red rectangles in Fig. 4(a), all sizes of 256×256 pixels, are shown in Fig. 5. ROI #1 to ROI #4 are the text, low-density, low-contrast, and edge area, respectively. In general, three enhancement methods can individually offer a good visual effect. For ROI #1, the text presents more brightly and clearly using LP_DUM. ROI #2 shows that LP_DUM can efficiently identify low-density regions and sharpen the edges.
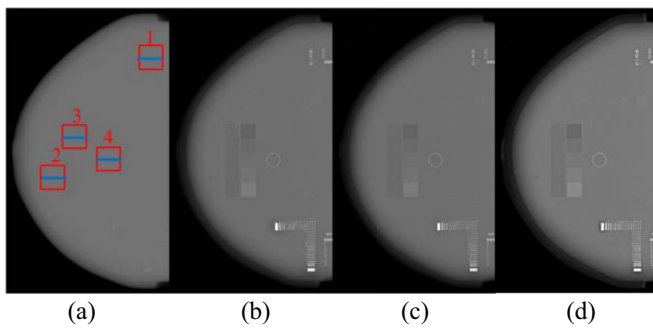
Fig. 4. Comparison of processed phantom data by different methods. (a) Origin. Enhanced image by (b) UM, (c) LPE, and (d) LP_DUM.
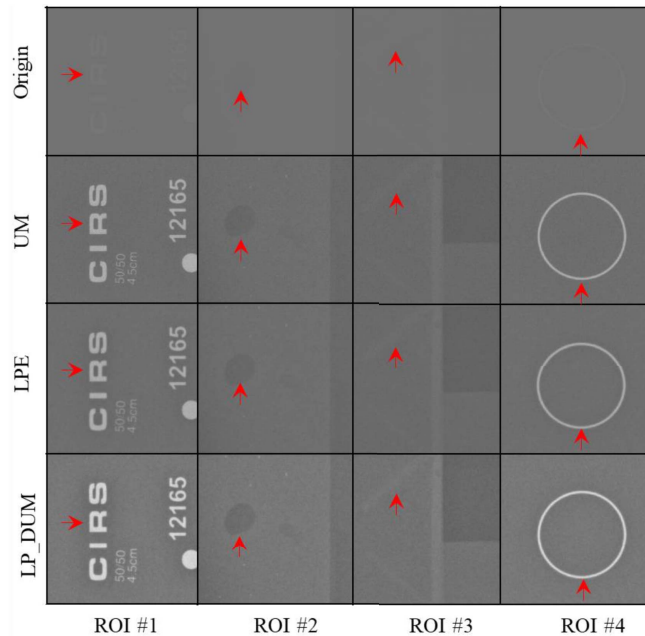

Fig. 5. Regions cropped from Fig. 4. First row to last row are regions cropped from the original image, processed image by UM, LPE, and LP_DUM, respectively. Red arrows indicate where LP_DUM works well.

In addition, it can be found that the calcifications are more easily recognizable in enhanced results, when compared to UM and LPE methods. ROI #3 shows that the direction of the fiber is clearer with LP_DUM. For ROI #4, the image is considerably brighter and the edges are clear using LP_DUM. The window/level set for each ROI are same.

Fig. 6 presents the image intensity profiles of the middle row (blue line) of four red squares. Through the profile, the contrast of images is improved whether UM, LPE, or LP_DUM methods compared with original phantom image. And LP_DUM is superior to the other two methods with the largest amplitude of curves in the feature areas in terms of improving image contrast. Furthermore, the invariably highest grayscale of LP_DUM implies the brightest abnormal regions (e.g., masses or micro-calcifications), which are more discriminable for diagnosis.

Table I shows the IE value comparison of the entire image and four ROIs images. The LP_DUM algorithm has the largest IE in the global and local images, thereby indicating the presence of substantial information.
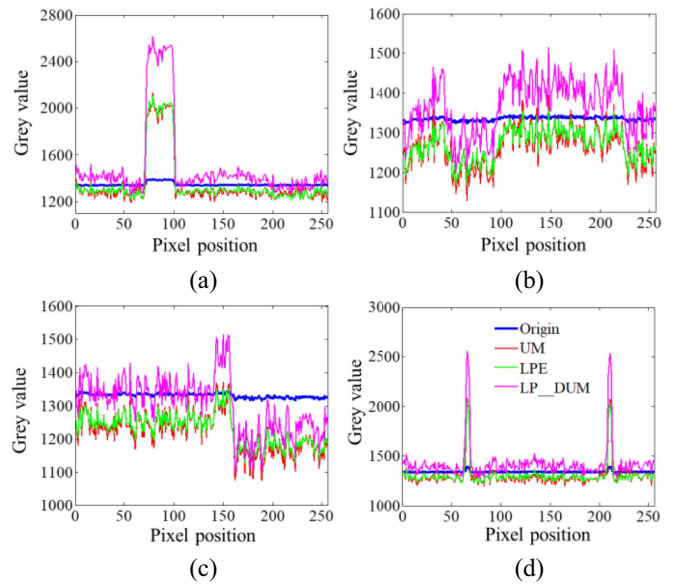

Fig. 6. Profiles comparison of ROIs. (a) ROI #1. (b) ROI #2. (c) ROI #3. (d) ROI #4.

TABLE I
IE OF ENHANCED PHANTOM IMAGE BY THREE METHODS

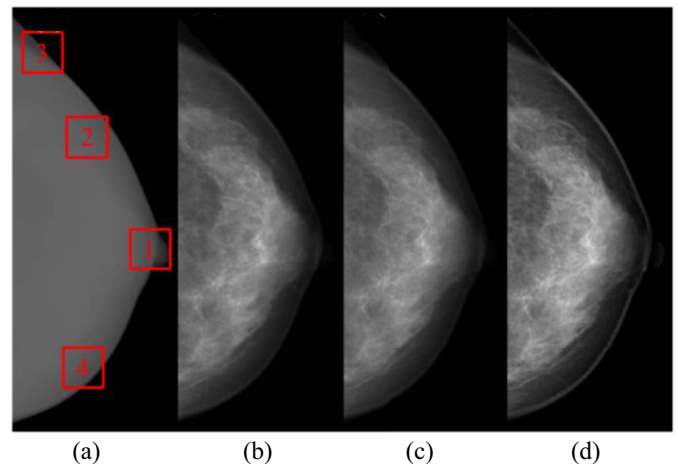| Selected Area	Entire Image	ROI #1	ROI #2	ROI #3	ROI #4
UM	1.89	0.21	0.03	0.41	0.26
LPE	1.89	0.18	0.01	0.25	0.29
LP_DUM	2.38	0.95	0.92	0.54	1.22

Fig. 7. Comparison of processed heterogeneously dense breast images by different methods. (a) Origin. Enhanced image by (b) UM, (c) LPE, and (d) LP_DUM.

B. Realistic Breast Data

1) Enhanced Mammogram of Heterogeneously Dense Breast: Fig. 7 shows enhancement results of the heterogeneously dense breast. Subjectively, LP_DUM enhancement method provides much clearer contrast/shape/details of the mammary gland. In addition, the edge of the skin is well-preserved with the LP_DUM method.
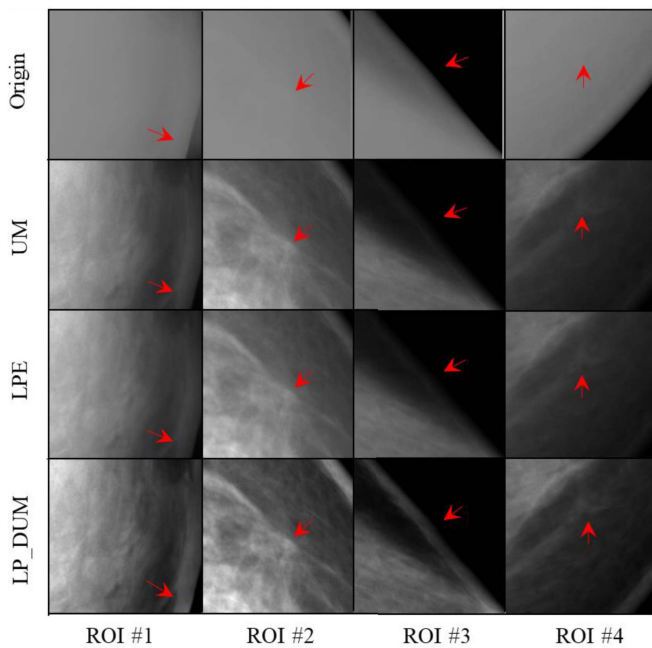
Fig. 8. Regions cropped from Fig. 7. First row to last row are regions cropped from the original image, processed image by UM, LPE, and LP_DUM, respectively.

TABLE II
OBJECTIVE INDEXES OF ENHANCEMENT DENSE MAMMOGRAMS IN ROIS

Selected Area	UM		LPE		LP_DUM	
	IE	PSNR	IE	PSNR	IE	PSNR
ROI#1	2.46	10.67	2.48	10.45	2.67	11.14
ROI#2	2.15	11.18	2.20	11.07	2.43	11.61
ROI#3	1.81	6.39	1.81	5.93	1.82	7.37
ROI#4	2.36	10.93	2.43	10.63	2.46	11.22

Fig. 8 shows the magnification of four regions cropped from Fig. 7. ROI #1 shows that the tissue texture cannot be identified with the UM and LPE, whereas evident subtle structure are shown by LP_DUM. ROI #2 shows a clear breast texture, thereby enabling doctors to easily identify mammary nodules. The edge is well-preserved in ROI #3 with LP_DUM, but poor edge information exists in the UM and LPE methods. The result of ROI #4 is consistent with the three ROIs.

IE and PSNR of four regions are listed in Table II for enhanced results of dense breast. Through this table, it can be seen that the IE and PSNR of all regions with LP_DUM are higher than that of the other two methods. These objective indexes indicate LP_DUM has better enhancement and noise suppression performance.

2) Enhanced Mammogram With Calcifications: Fig. 9 shows enhanced results of mammogram with calcifications. It can be seen that the fine details are distinctly improved by LP_DUM, and the calcification clusters are more discriminable. These enhancement results are useful for computer-aided diagnosis systems to automatically segment the abnormal regions in mammograms with breast cancer.

Fig. 10 shows the four enhanced regions cropped from Fig. 9. ROI #1 shows that the nipple almost cannot be
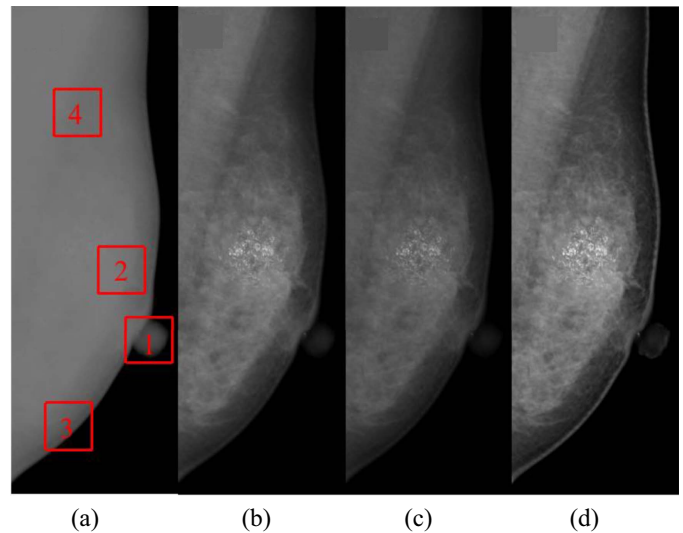

Fig. 9. Comparison of processed mammograms with calcification by different methods. (a) Origin. Enhanced image by (b) UM, (c) LPE, and (d) LP_DUM.
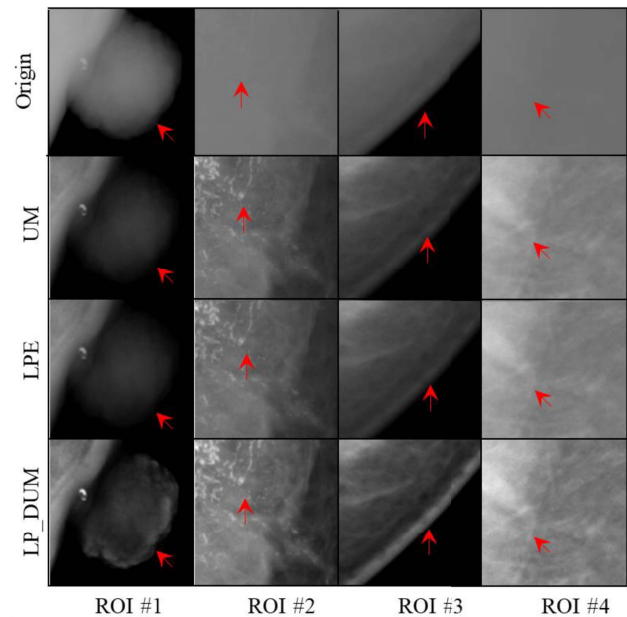

Fig. 10. Regions cropped from Fig. 9. First row to last row are regions cropped from the original image, processed image by UM, LPE, and LP_DUM, respectively.

identified with the UM and LPE, whereas evident subtle structure are shown by LP_DUM. ROI #2 displays enhanced calcification clusters, and LP_DUM can highlight calcification with a more satisfactory contrast between abnormal and normal regions. The skin edge is well-preserved in ROI #3 with LP_DUM. In ROI #4, LP_DUM can make pectoral muscle very layered, which is significant for accurate pectoral segmentation.

IE and PSNR of four regions are listed in Table III for enhancement mammograms with calcification. It can be seen that the IE and PSNR of almost regions with LP_DUM are highest. Although in ROI #2, PSNR is slightly lower than other methods, considering that the region is a micro-calcification cluster, such lower PSNR is also reasonable.

TABLE III
OBJECTIVE INDEXES OF ENHANCEMENT MAMMOGRAMS
WITH CALCIFICATIONS IN ROIs

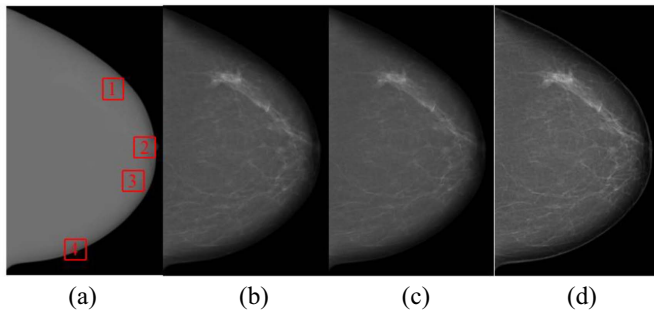| Selected Area	UM		LPE		LP_DUM	
	IE	PSNR	IE	PSNR	IE	PSNR
ROI#1	1.92	11.40	1.85	11.22	2.03	15.18
ROI#2	2.64	21.34	2.63	21.23	3.01	18.38
ROI#3	2.04	12.25	2.08	11.76	2.20	12.78
ROI#4	1.24	16.23	1.15	16.25	1.77	16.57

Fig. 11. Comparison of processed mammogram of fatty breast by different methods. (a) Origin. Enhanced image by (b) UM, (c) LPE, and (d) LP_DUM.
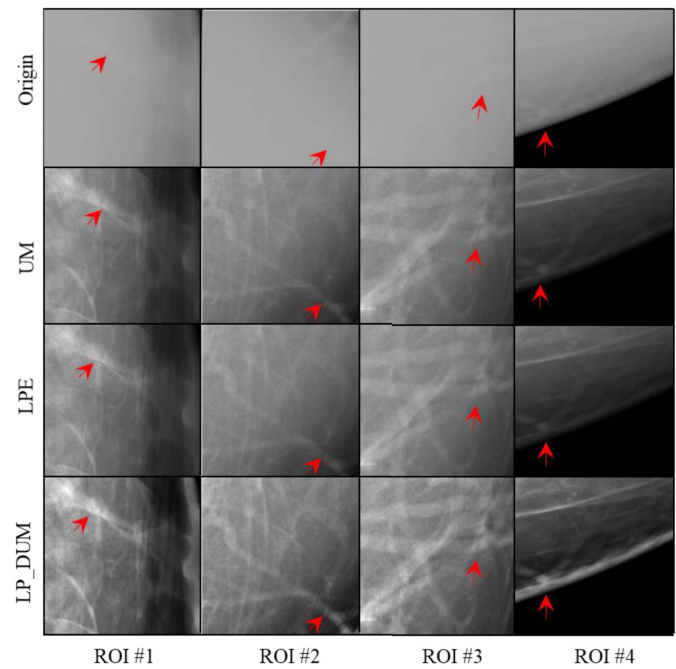

Fig. 12. Regions cropped from Fig. 11. First row to last row are regions cropped from the original image, processed image by UM, LPE, and LP_DUM, respectively.

3) Mammogram Enhancement With Fatty Tissue Predominating: Fig. 11 shows enhancement results of mammogram with fatty tissue predominating, which is suspected with infiltrating ductal carcinoma. Excellent visual mammary ducts and microvascular are acquired and fine shin edge is well-preserved with LP_DUM. Furthermore, the gray level range of suspicious abnormal region is highlighted. In this way, the improvement is valuable to a radiologist or nonradiologist reader for understanding those suspicious abnormalities.

Four enhanced ROIs are shown in Fig. 12. ROI #1 shows the suspicious abnormal region are improved with LP_DUM enhancement, whereas ambiguous mammary marginal are shown by UM and LPE. ROI #2 displays enhanced microvascular with a more satisfactory pattern. The result of ROI #3 is consistent with ROI #2. The skin edge is well-preserved in ROI #4 with LP_DUM.

Objective indexes of enhancement mammograms of fatty breast in ROIs are listed in Table IV. The LP_DUM method has a significantly larger IE and SNR value than those of the other two methods; hence, the former is a good option to acquire satisfactory enhancement effects of the edge and mammary ducts.

TABLE IV
OBJECTIVE INDEXES OF ENHANCEMENT MAMMOGRAMS
OF FATTY BREAST IN ROIs

Selected Area	UM		LPE		LP_DUM	
	IE	PSNR	IE	PSNR	IE	PSNR
ROI#1	2.44	11.84	2.43	11.45	2.55	13.07
ROI#2	1.89	11.48	1.92	11.17	2.08	12.45
ROI#3	1.98	14.91	1.97	14.69	2.17	16.15
ROI#4	1.97	7.57	1.97	7.29	2.09	9.10

IV. DISCUSSION

This paper developed a multiscale contrast enhancement using LP_DUM to enhance the contrast and highlight the edges of mammograms as well as suppress noise. This method first decomposes an image into multilevel subimages, and DUM enhancement are performed in each scale. This method introduces the global mean, neighborhood mean, and neighborhood variance to dynamically adjust the weight factor instead of fixed parameter in the UM enhancement.

Consequently, pixels in different positions are enhanced adaptively. For the phantom data and realistic experiments, the proposed enhancement method can qualitatively and quantitatively obtain a satisfactory image. High contrast is beneficial in detecting abnormal lesions like masses or micro-calcifications, while distinct mammary gland can avoid ambiguous blocks in images. In addition, the higher PSNR indicates noise was suppressed with LP_DUM, at least compared with UM and LPE.

Theoretically, the more levels of LP are deconstructed, the greater degree of the image is enhanced. However, limited beneficial information of low-resolution image can provide for enhancement due to the utilization of Gaussian low-pass filter at each LP scale. The amount of calculation increases significantly due to the DUM enhancement on each LP level. Thus, we decomposed the image to the fourth level. Similarly, considering the computation efficiency and enhancement effect, the size of the neighborhood is chosen 11×11 for efficient enhancement.

The selection and determination of some parameters used in analytical considerations should be rational. Two adjustable

weight parameters lead to satisfactorily enhanced results for different images, that is, α in DUM and k_n in the image restoration processing. Users can experimentally select their optimal value to qualitatively and quantitatively obtain the best enhancement results. Moreover, α as a sharpening factor determines the effect of the global mean that controls the DUM enhancement. The typical value of 0.6 in experiments substantially maintains the details and artifacts without any increase. The parameter k_n determines the proportion of high-frequency components that accounts for the recovery image. We can select different values for various levels or different values for various pixels but in the same level. In this paper, we simplified the experiment by selecting three constants (i.e., 1.8, 1.8, and 1.0) for four levels from the lower to the upper resolution images.

Nevertheless, there are still some limitations in this paper. First, the number of mammogram in our experiment is small, although three typical realistic breast data has been enhanced with excellent contrast and edge preservation. It is not proven that LP_DUM can aid in enhancing other breast lesions (such as masses just presented in phantom data), which should actually be the final goal of the increase of image quality. Accordingly, the enhanced results are insufficient to demonstrate the superiority of the proposed method in practical applications. Second, due to the processing noise correlations arise which will slightly affect clinical performance. The impact of this correlation can be observed in Fig. 10 ROI #2. In this figure, we can see that separate structures become a little connected using the LP_DUM algorithm. Third, in Fig. 10 ROI #1, it can also be seen that the nipple seems to be separate from the breast. Although better contrast inside the nipple can be depicted, there is still a question if it is appropriate that the nipple becomes disconnected. Fourth, generally, phantom data is often used for imaging quality analysis. Here, we utilize it to evaluate the enhancement effect. Compared with UM and LPE, the contrast of phantom data did not improved significantly using LP_DUM as shown in Figs. 4 and 5. However, in the realistic breast data, the enhanced performance of LP_DUM is indeed significantly better than UM and LPE as shown as Figs. 7–12. In realistic applications, the object to be enhanced is the realistic breast data instead of the phantom data. In general, LP_DUM is superior to the other two methods.

In addition, it must be explained that the use of IE measures of gray level distribution as measures of local contrast enhancement maybe not particularly meaningful for mammogram images [25]. Even though in many literatures lots of evaluation indexes have been presented [14], [27], there is no reliable basis for the effectiveness of these indexes. The subjective evaluation of radiologist reader is the most significant method for mammogram enhancement. A quantitative evaluation criterion is lacking to precisely measure the enhancement effect. Further work might involve proposing more reliable evaluation indexes, in the aim to be consistent with the subjective evaluation.

V. CONCLUSION

The proposed integrated method, which has been tested in phantom and realistic date experiments, shows great potential to adaptively enhance the details and suppress the noise of digital mammography.

REFERENCES

[1] A. H. Alasadi and A. K. Al-Saedi, "A method for microcalcifications detection in breast mammograms," *J. Med. Syst.*, vol. 41, no. 4, p. 68, 2017.

[2] K. Panetta, Y. Zhou, S. Agaian, and H. Jia, "Nonlinear unsharp masking for mammogram enhancement," *IEEE Trans. Inf. Technol. Biomed.*, vol. 15, no. 6, pp. 918–928, Nov. 2011.

[3] K. A. Panetta, E. J. Wharton, and S. S. Agaian, "Human visual system-based image enhancement and logarithmic contrast measure," *IEEE Trans. Syst., Man, Cybern. B, Cybern.*, vol. 38, no. 1, pp. 174–188, Feb. 2008.

[4] F. Zanca *et al.*, "Evaluation of clinical image processing algorithms used in digital mammography," *Med. Phys.*, vol. 36, no. 3, pp. 765–775, 2009.

[5] L. M. Warren *et al.*, "The effect of image processing on the detection of cancers in digital mammography," *Amer. J. Roentgenol.*, vol. 203, no. 2, pp. 387–393, 2014.

[6] Q. Wang and R. K. Ward, "Fast image/video contrast enhancement based on weighted thresholded histogram equalization," *IEEE Trans. Consum. Electron.*, vol. 53, no. 2, pp. 757–764, May 2007.

[7] J. A. Stark, "Adaptive image contrast enhancement using generalizations of histogram equalization," *IEEE Trans. Image Process.*, vol. 9, no. 5, pp. 889–896, May 2000.

[8] A. Polesel, G. Ramponi, and V. J. Mathews, "Image enhancement via adaptive unsharp masking," *IEEE Trans. Image Process.*, vol. 9, no. 3, pp. 505–510, Mar. 2000.

[9] G. Ramponi, "A cubic unsharp masking technique for contrast enhancement," *Signal Process.*, vol. 67, no. 2, pp. 211–222, 1998.

[10] G. Deng, "A generalized unsharp masking algorithm," *IEEE Trans. Image Process.*, vol. 20, no. 5, pp. 1249–1261, May 2011.

[11] S. Das and M. K. Kundu, "A neuro-fuzzy approach for medical image fusion," *IEEE Trans. Biomed. Eng.*, vol. 60, no. 12, pp. 3347–3353, Dec. 2013.

[12] H. Deng *et al.*, "Mammogram enhancement using intuitionistic fuzzy sets," *IEEE Trans. Biomed. Eng.*, vol. 64, no. 8, pp. 1803–1814, Aug. 2017.

[13] F. Russo, "Recent advances in fuzzy techniques for image enhancement," *IEEE Trans. Instrum. Meas.*, vol. 47, no. 6, pp. 1428–1434, Dec. 1998.

[14] A. Laine, J. Fan, and W. Yang, "Wavelets for contrast enhancement of digital mammography," *IEEE Eng. Med. Biol. Mag.*, vol. 14, no. 5, pp. 536–550, Sep./Oct. 1995.

[15] X. Bai, F. Zhou, and B. Xue, "Image enhancement using multi scale image features extracted by top-hat transform," *Opt. Laser Technol.*, vol. 44, no. 2, pp. 328–336, 2012.

[16] S. Dippel, M. Stahl, R. Wiemker, and T. Blaffert, "Multiscale contrast enhancement for radiographies: Laplacian pyramid versus fast wavelet transform," *IEEE Trans. Med. Imag.*, vol. 21, no. 4, pp. 343–353, Apr. 2002.

[17] A. Mencatini, M. Salmeri, R. Lojacono, M. Frigerio, and F. Caselli, "Mammographic images enhancement and denoising for breast cancer detection using dyadic wavelet processing," *IEEE Trans. Instrum. Meas.*, vol. 57, no. 7, pp. 1422–1430, Jul. 2008.

[18] X. Liu, J. Tang, S. Xiong, Z. Feng, and Z. Wang, "A multiscale contrast enhancement algorithm for breast cancer detection using Laplacian pyramid," in *Proc. Int. Conf. Inf. Autom.*, 2009, pp. 1167–1171.

[19] D. G. Lowe, "Distinctive image features from scale-invariant keypoints," *Int. J. Comput. Vis.*, vol. 60, no. 2, pp. 91–110, 2004.

[20] P. Burt and E. Adelson, "The Laplacian pyramid as a compact image code," *IEEE Trans. Commun.*, vol. COM-31, no. 4, pp. 532–540, Apr. 1983.

[21] K. Bliznakova *et al.*, "Experimental validation of a radiographic simulation code using breast phantom for X-ray imaging," *Comput. Biol. Med.*, vol. 40, no. 2, pp. 208–214, 2010.

[22] J. Wang *et al.*, "Discrimination of breast cancer with microcalcifications on mammography by deep learning," *Sci. Rep.*, vol. 6, Jun. 2016, Art. no. 27327.

[23] H. Li, K. J. R. Liu, and S.-C. B. Lo, "Fractal modeling and segmentation for the enhancement of microcalcifications in digital mammograms," *IEEE Trans. Med. Imag.*, vol. 16, no. 6, pp. 785–798, Dec. 1997.

[24] S. S. Agaian, B. Silver, and K. A. Panetta, "Transform coefficient histogram-based image enhancement algorithms using contrast entropy," *IEEE Trans. Image Process.*, vol. 16, no. 3, pp. 741–758, Mar. 2007.

[25] W. M. Morrow, R. B. Paranjape, R. M. Rangayyan, and J. E. L. Desautels, "Region-based contrast enhancement of mammograms," *IEEE Trans. Med. Imag.*, vol. 11, no. 3, pp. 392–406, Sep. 1992.

[26] Q. Huynh-Thu and M. Ghanbari, "Scope of validity of PSNR in image/video quality assessment," *Electron. Lett.*, vol. 44, no. 13, pp. 800–801, Jun. 2008.

[27] J. Tang, X. Liu, and Q. Sun, "A direct image contrast enhancement algorithm in the wavelet domain for screening mammograms," *IEEE J. Sel. Topics Signal Process.*, vol. 3, no. 1, pp. 74–80, Feb. 2009.